Jordanian Journal of Computers and Information Technology (JJCIT), Vol. 12, No. 03, September 2026.

ANALYTICAL INSIGHTS INTO THE AVERAGE BLOCK ERROR RATE OF FLUID ANTENNA SYSTEMS UNDER SHORT-PACKET CONSTRAINTS

Chi-Bao Le and Tin Phu Tran

(Received: 22-Apr.-2026, Revised: 12-Jun.-2026, Accepted: 29-Jun.-2026)

ABSTRACT

Fluid antenna systems (FASs) offer immense spatial diversity within compact spaces. However, existing performance analyses predominantly rely on Shannon's capacity bounds, assuming infinite blocklength transmissions. To address the strict requirements of emerging Internet-of-Things (IoT) and ultra-reliable low-latency communications (URLLCs), this paper investigates a point-to-point FAS under short-packet communication (SPC) constraints. We rigorously derive closed-form analytical expressions for the average block error rate (BLER), effective system throughput and reliability. Furthermore, we conduct an asymptotic analysis in the high signal-to-noise ratio (SNR) regime, mathematically revealing that the system's diversity order is strictly determined by the rank of the spatial correlation matrix. Extensive Monte Carlo simulations validate the high accuracy of our proposed analytical models, demonstrating that increasing the number of fluid ports drastically reduces the BLER.

KEYWORDS

Fluid antenna systems, Short-packet communications, Block error rate, Ultra-reliable low-latency communications, Throughput, Reliability.

1. INTRODUCTION

The rapid proliferation of the Internet-of-Things (IoT) and the stringent demands of ultra-reliable and low-latency communications (URLLC) have driven a paradigm shift in wireless network design [1][2][3]. In emerging applications, such as industrial automation, remote healthcare and autonomous systems, devices typically exchange short control commands or status updates rather than large data payloads. These scenarios require transmitting small data packets within strict millisecond-level latency constraints while ensuring near-perfect reliability [4].

Under such strict latency requirements, the classic Shannon capacity theory, which assumes infinitely long data blocks to achieve an arbitrarily low error rate, becomes inadequate [5]. For short-packet communications (SPCs), the blocklength is finite, making the probability of decoding errors non-negligible. This fundamental physical limitation is addressed by the finite blocklength information theory pioneered by [6]-[8], which mathematically characterizes the block error rate (BLER) for short packets. Consequently, the research community has extensively re-evaluated various wireless technologies, ranging from massive multiple-input multiple-output (MIMO) [9]-[11] to intelligent reflecting surfaces [12]-[14], strictly through the lens of SPC. Furthermore, while initial studies evaluated short-packet communications assuming independent fading channels, recent advancements have extended the finite blocklength-information theory to correlated fading environments [15] to better contextualize practical deployment scenarios.

Parallel to these theoretical advancements, the fluid antenna system (FAS) has emerged as a revolutionary hardware technology for compact devices [16]-[18]. Traditional MIMO systems require physical separation (typically at least half a wavelength) between antennas to ensure independent fading channels, which is impractical for small form-factor devices due to severe mutual coupling [19]. FAS overcomes this physical limitation by utilizing liquid metal or reconfigurable pixel structures, allowing a single radiating element to dynamically switch its position to the most favorable location (port) within a highly confined space [20]-[21]. By exploiting the spatial variations of the fading channel, FAS achieves significant spatial diversity without requiring multiple bulky and power-hungry radio frequency (RF) chains.

C.-B. Le (Corresponding Author) and T. P. Tran are with Faculty of Information Technology, Ton Duc Thang University, Ho Chi Minh City, Vietnam. Emails: lechibao@tdtu.edu.vn and phutrantin@tdtu.edu.vn

While a growing body of literature has investigated the theoretical performance limits of FAS, typically employing Jakes' fading model to characterize the strong spatial correlation among densely packed ports [22], these studies predominantly rely on the infinite blocklength assumption. Very recently, the critical interplay between FAS and SPC has begun to attract attention. For instance, the authors in [23] investigated a UAV-enabled relaying network equipped with FAS under short-packet constraints. Despite this pioneering effort, their work primarily targets energy-efficiency optimization within a complex relaying topology under Nakagami-m fading. Beyond this, other recent studies, such as [24], have investigated the performance of FAS under finite blocklength constraints in multi-user setups. Currently, a comprehensive, exact and tractable analytical framework characterizing the reliability and throughput of a baseline point-to-point (P2P) FAS link under SPC constraints is still missing from the literature, even though such a baseline setup serves as the essential building block for more complex networks.

Motivated by this critical research gap, this paper comprehensively analyzes the delivery performance of a P2P FAS link operating under strict SPC constraints. The main contributions of our work are summarized as follows:

- We formulate a comprehensive mathematical system model that elegantly integrates the highly correlated spatial fading environment of the FAS with the finite blocklength constraints of SPC.
- We derive highly accurate, closed-form expressions for the exact average BLER, the effective system throughput and the overall system reliability. This is achieved by exploiting the inclusion-exclusion principle and eigenvalue decomposition (EVD) to evaluate the cumulative distribution function (CDF) of the effective SNR, combined with a linear approximation to bypass the analytically complex Gaussian Q-function.
- To gain deeper fundamental insights, we conduct an asymptotic analysis of the system performance in the high-SNR regime. This rigorous approach explicitly reveals the exact diversity order of the FAS link, mathematically demonstrating how the rank of the spatial correlation matrix fundamentally dictates the achievable reliability.
- We investigate the optimal design of blocklength allocation to maximize the effective system throughput under strict reliability and latency boundaries, providing vital operational insights for the physical implementation of short-packet FAS.
- We provide extensive Monte Carlo simulations to definitively validate the accuracy of our derived analytical models. The numerical results clearly illustrate the fundamental trade-offs among the number of fluid ports, the physical antenna space and the short-packet parameters in determining the overall system performance.

The rest of this paper is organized as follows. Section 2 describes the physical transmission framework and the spatially correlated channel model of the FAS. Section 3 presents the core mathematical derivations for the exact and asymptotic average BLER, as well as the effective system throughput and reliability, followed by an optimized short-packet blocklength design framework. Section 4 provides comprehensive numerical results to validate our proposed analytical models and finally, Section 5 concludes the paper.

Notation: $\Pr(\cdot)$ denotes probability; $\mathbb{E}\{\cdot\}$ is the expectation operator; $J_0(\cdot)$ is the zero-order Bessel function of the first kind; $Q(\cdot)$ is the standard Gaussian Q-function; $(\cdot)^T$ and $(\cdot)^H$ denote the transpose and conjugate transpose operations, respectively.

2. System Model

2.1 Signal Transmission and FAS Topology

The fundamental limits of fluid antenna systems (FASs) have been actively investigated in recent literature. For instance, a rigorous geometric framework connecting the spatial diversity order directly to the rank of the correlation matrix was established in [25]. Furthermore, the practical deployment of FASs in 6G ultra-reliable communications must account for practical hardware non-idealities, such as the inherent trade-off between the total port count and the effective transmission blocklength caused by non-negligible port-switching delays [26]. More recently, the performance limits of FASs have been

extended to cooperative relay topologies under finite-blocklength constraints, including unmanned aerial vehicle (UAV) networks [27].

Consider a point-to-point wireless link comprising a single-antenna transmitter and a receiver equipped with a one-dimensional fluid antenna structure. The physical space allocated for the fluid antenna has a normalized length of L_s (measured in terms of the carrier wavelength). For digital-processing tractability, we assume that the receiver uniformly discretizes this continuous space into K predefined ports along L_s. Due to hardware constraints, the receiver possesses only a single active RF chain. However, it is capable of dynamically switching this RF chain to whichever of the K ports currently offers the highest signal quality.

Suppose that the transmitter sends a signal x with an average transmit power of P. The received baseband signal at the k-th port ($k \in \{1,2,\dots,K\}$) is given by:

$$y_k = \sqrt{P} h_k x + n_k, \tag{1}$$

where $h_k \sim \mathcal{CN}(0,1)$ is the complex Rayleigh flat-fading channel coefficient between the transmitter and the k-th port and $n_k \sim \mathcal{CN}(0,\sigma^2)$ represents the additive white Gaussian noise (AWGN) at the receiver with variance σ^2.

The instantaneous SNR at the k-th port is defined as $\gamma_k = \rho|h_k|^2$, where $\rho = P/\sigma^2$ is the average transmit SNR. Since the FAS controller aims to maximize the system performance, the effective SNR available for decoding the incoming packet is the maximum across all available ports:

$$\Gamma = \max_{k\in\{1,\dots,K\}} \gamma_k. \tag{2}$$

It is worth noting that the formulation in (2) relies on the assumptions of perfect channel-state information (CSI) and instantaneous port selection. In practical FAS deployments, however, hardware non-idealities, such as channel estimation overhead and mechanical/electronic RF switching delays, present notable constraints [26]. Crucially, since the system operates under SPC with a strictly limited finite blocklength, any non-negligible switching delay directly penalizes the system by reducing the effective number of channel uses available for data payload transmission. While a comprehensive analysis of these hardware impairments is beyond the scope of this baseline study, the idealized model under perfect CSI serves as an indispensable theoretical benchmark that establishes the fundamental performance upper bounds, which is a widely adopted approach in recent short-packet multi-antenna literature [34].

2.2 Spatial Correlation Characterization

Since the K ports are densely packed into a confined physical space L_s, the channel fading coefficients $h_1, h_2, \dots, h_K$ are highly correlated. Assuming a rich scattering environment, which is typical in dense IoT deployments, the spatial correlation between the fading envelopes of the i-th and j-th ports can be characterized by Jakes' fading model [28]. The spatial correlation coefficient is mathematically expressed as:

$$r_{i,j} = J_0\left(2\pi \frac{|i-j|}{K-1} L_s\right). \tag{3}$$

These pairwise coefficients constitute a $K \times K$ spatial correlation matrix, denoted as $\mathbf{R}$, where its (i,j)-th entry is $[\mathbf{R}]_{i,j} = r_{i,j}$. We explicitly acknowledge that Jakes' model relies on an idealized isotropic scattering environment with a uniform angle of arrival (AoA), which constitutes a practical limitation, as it may not fully capture directional non-isotropic scattering, shadow fading or strong line-of-sight (LoS) components common in dense, cluttered IoT deployments. Nevertheless, the adoption of Jakes' model is rigorously justified, because it serves as the foundational mathematical benchmark in fluid-antenna literature [22], [29], enabling a tractable analytical baseline. Crucially, from a physical standpoint, isotropic scattering yields the highest possible spatial correlation among closely spaced ports. Therefore, analyzing the system under Jakes' model provides a conservative, robust "worst-case" performance baseline; if the FAS link can meet the strict reliability constraints under this extreme correlation, it will perform even better in realistic environments with directional scattering or LoS paths where correlation is naturally lower.

Directly analyzing the maximum of highly correlated random variables in (2) is mathematically

intractable. To facilitate the statistical analysis, we decouple these correlated channels into a set of independent ones by applying the eigenvalue decomposition (EVD) to the correlation matrix [30]-[31].

$$\mathbf{R} = \mathbf{U}\boldsymbol{\Lambda}\mathbf{U}^H, \tag{4}$$

where $\mathbf{U}$ is a unitary matrix containing the eigenvectors and $\boldsymbol{\Lambda} = \mathrm{diag}(\mu_1, \mu_2, \dots, \mu_K)$ is a diagonal matrix of the corresponding eigenvalues. The eigenvalues are arranged in a descending order, i.e., $\mu_1 \geq \mu_2 \geq \cdots \geq \mu_K \geq 0$. This mathematical transformation decouples the highly correlated fluid antenna channel vector $\mathbf{h}$ into a set of independent virtual variables *via* the linear relation $\mathbf{h} = \mathbf{U}\boldsymbol{\Lambda}^{1/2}\mathbf{g}$, where $\mathbf{g} \sim \mathcal{CN}(\mathbf{0}, \mathbf{I}_K)$ represents a vector of independent and identically distributed (i.i.d.) standard complex Gaussian random variables. Because $\mathbf{U}$ is a unitary matrix (i.e., $\mathbf{U}^H\mathbf{U} = \mathbf{I}_K$), this transformation completely diagonalizes the spatial correlation matrix while strictly preserving the total statistical properties and physical energy of the channel [28], [30]. Following this rigorous justification, retaining only the S dominant eigenvalues allows us to systematically reduce the system's dimensionality to its effective rank, ensuring mathematical tractability while retaining the underlying physical spatial-correlation characteristics [29].

Physically, when the space L_s is sufficiently small and the number of ports K is large, the matrix $\mathbf{R}$ becomes severely rank-deficient. Consequently, many of the smaller eigenvalues approach zero due to the extreme spatial correlation [29]. Let $S \leq K$ denote the effective rank of $\mathbf{R}$, meaning that there are only S dominant, non-zero eigenvalues $(\mu_1, \dots, \mu_S)$. This rank S dictates the true spatial degrees of freedom in the system and plays a pivotal role in the subsequent asymptotic analysis.

To formally quantify the effective rank S, we adopt a strict cumulative energy-fraction criterion. Specifically, the effective rank S is mathematically defined as the minimum number of dominant eigenvalues required to capture a significant fraction τ of the total spatial channel energy, expressed as:

$$S = \arg\min_{s} \left\{ \frac{\sum_{m=1}^{s} \mu_m}{\sum_{k=1}^{K} \mu_k} \geq \tau \right\}, \tag{5}$$

where τ is a pre-defined threshold close to unity (e.g., $\tau = 99.9\%$). This criterion guarantees that the truncated smaller eigenvalues have a mathematically negligible impact on the overall distribution accuracy while maintaining a rigorous framework for the asymptotic diversity-order analysis.

3. Performance Analysis: Average BLER

In this section, we derive the statistical properties of the maximum SNR Γ. Subsequently, we incorporate the finite blocklength Q-function to obtain the exact average BLER and its asymptotic bound.

3.1 Exact Statistical Characterization of Γ

By leveraging the EVD transformation in (C.5) and the inclusion-exclusion principle, the CDF of the effective SNR Γ for the P2P FAS can be tightly approximated as a finite sum of exponential functions [29]:

$$F_\Gamma(\gamma) \approx 1 + \sum_{k=1}^{S} (-1)^k \sum_{\mathcal{N}_k} \exp\left(-\frac{\gamma}{\rho}\Delta_k\right), \tag{6}$$

where S is the effective rank of $\mathbf{R}$ and $\sum_{\mathcal{N}_k}$ denotes the summation over all possible combinations of k distinct indices $(n_1, n_2, \dots, n_k)$ chosen from the set $\{1,2, \dots, S\}$. The term Δ_k represents the sum of the reciprocals of the chosen eigenvalues:

$$\Delta_k = \sum_{j=1}^{k} \frac{1}{\mu_{n_j}}. \tag{7}$$

3.2 Average BLER Formulation

We now incorporate the short-packet constraints. Suppose that the transmitter sends a packet containing D information bits over a finite blocklength of L channel uses, yielding a nominal coding rate of $R_c = D/L$ (bits per channel use).

Jordanian Journal of Computers and Information Technology (JJCIT), Vol. 12, No. 03, September 2026.

According to the finite-blocklength information theory [32], the instantaneous BLER for a specific SNR realization Γ is closely approximated by the Gaussian Q-function

$$\epsilon(\Gamma) \approx Q\left(\sqrt{\frac{L}{V(\Gamma)}}(\log_2(1+\Gamma) - R_c)\right), \tag{8}$$

where $V(\Gamma) = (1-(1+\Gamma)^{-2})(\log_2 e)^2$ is the channel dispersion [33]. To evaluate the system reliability, the average BLER is obtained by taking the mathematical expectation of (8) over the distribution of Γ:

$$\bar{\epsilon} = \mathbb{E}[\epsilon(\Gamma)] = \int_0^\infty \epsilon(x) f_\Gamma(x) dx \tag{9}$$

where $f_\Gamma(x)$ is the probability-density function (PDF) of Γ.

Evaluating (9) directly is mathematically intractable due to the complex Q-function. To resolve this, we adopt a widely accepted linear approximation for the Q-function [23]. Let $\theta = 2^{R_c} - 1$ be the target SNR threshold required to support the rate R_c. The Q-function can be linearized around θ as:

$$\epsilon(x) \approx \begin{cases} 1, & x < a \\ \frac{1}{2} - \beta(x-\theta), & a \le x \le b \\ 0, & x > b \end{cases} \tag{10}$$

where the slope β and the boundaries a, b are defined as:

$$\beta = \sqrt{\frac{L}{2\pi V(\theta)}}, \tag{11}$$

$$a = \theta - \frac{1}{2\beta}, b = \theta + \frac{1}{2\beta}. \tag{12}$$

To justify the accuracy of this piece-wise linear model and quantify the approximation error, we refer to the analytical-integration framework recently established in [34]. Specifically, by applying integration by parts to the average BLER expectation, the piece-wise boundaries logically cancel out the CDF evaluations at the limits. Similar to the exact formulation derived in [34], Eq. (11), the average BLER elegantly simplifies to:

$$\bar{\epsilon} = \int_0^\infty \epsilon(x) f_\Gamma(x) dx \approx \beta \int_a^b F_\Gamma(x) dx \tag{13}$$

The maximum approximation error occurs only near the transition boundaries a and b. In the targeted ultra-reliable regime characterized by high average SNR ($\rho \to \infty$), the operational transition interval $[a, b]$ becomes extremely narrow relative to the total dynamic range of Γ. Consequently, the integration error introduced outside this interval decays exponentially toward zero, rendering this linear approximation mathematically sound, exceptionally tight and highly reliable for asymptotic performance evaluations in short-packet networks.

By exploiting this piecewise linear model, we derive a tractable, closed-form expression for the average BLER.

Theorem 1 Under SPC constraints, the exact average BLER of the FAS link is tightly approximated by:

$$\bar{\epsilon} \approx 1 + \sum_{k=1}^{S} (-1)^k \sum_{\mathcal{N}_k} \frac{\beta\rho}{\Delta_k} \left(e^{-\frac{a\Delta_k}{\rho}} - e^{-\frac{b\Delta_k}{\rho}} \right). \tag{14}$$

Proof: The proof is provided in Appendix A.

3.3 Asymptotic Analysis and Diversity Order

To gain deeper fundamental insights into the system limits, we perform an asymptotic analysis in the high-SNR regime ($\rho \to \infty$).

Theorem 2 In the high-SNR regime ($\rho \to \infty$), the average BLER of the FAS system decays asymptotically according to:

$$\bar{\epsilon}^{\infty} \approx \frac{\beta}{S+1}\left(\frac{1}{\prod_{i=1}^{S} \mu_i}\right)\left(\frac{1}{\rho}\right)^{S} (b^{S+1} - a^{S+1}). \tag{15}$$

Consequently, the diversity order of the FAS system under SPC is exactly equal to S, the rank of the spatial correlation matrix.

Proof: The asymptotic expansion is derived in Appendix B and its mathematically rigorous proof based on exact channel gain bounds and the Squeeze Theorem is detailed in Appendix C.

Remark 1 In a traditional MIMO system with K independent antennas, the diversity order is strictly K. However, due to the severe spatial correlation in FAS, the effective number of independent paths is bounded by S. Even if the number of ports K approaches infinity within a fixed space L_s, the diversity order S will eventually saturate, highlighting the fundamental physical limit of the FAS configuration.

3.4 Effective System Throughput Analysis

Beyond the system reliability evaluated by the average BLER, another crucial performance metric in short-packet communications is the effective system throughput. In the finite-blocklength regime, the throughput is defined as the expected fraction of information bits successfully delivered to the receiver per channel use.

Given that the transmitter sends D information bits over a blocklength of L channel uses, the nominal coding rate is $R_c = D/L$ (bpcu). Taking into account the transmission-failure probability characterized by the average BLER $\bar{\epsilon}$, the effective system throughput, denoted as η, can be formulated as [32]:

$$\eta = R_c(1 - \bar{\epsilon}) = \frac{D}{L}(1 - \bar{\epsilon}). \tag{16}$$

By substituting the exact average BLER derived in Theorem 1 into (16), we obtain the exact closed-form expression for the effective system throughput of the FAS link:

$$\eta \approx R_c \left[1 + \sum_{k=1}^{S} (-1)^k \sum_{\mathcal{N}_k} \frac{\beta\rho}{\Delta_k}\left(e^{-\frac{a\Delta_k}{\rho}} - e^{-\frac{b\Delta_k}{\rho}}\right)\right]. \tag{17}$$

Furthermore, utilizing the asymptotic BLER from Theorem 2, the high-SNR asymptotic throughput can be straightforwardly expressed as:

$$\eta^{\infty} \approx R_c \left[1 - \frac{\beta}{S+1}\left(\frac{1}{\prod_{i=1}^{S} \mu_i}\right)\left(\frac{1}{\rho}\right)^{S} (b^{S+1} - a^{S+1})\right]. \tag{18}$$

Remark 2 It is worth noting that the effective system throughput definition in (16) serves as an optimistic physical-layer performance boundary, as it explicitly omits packet retransmissions and queueing delays. In practical URLLC deployments characterized by bursty traffic arrivals and finite-buffer dynamics, packet-drop policies and automatic repeat request (ARQ) overheads would introduce additional queueing delays and latency violations. Incorporating these finite-buffer cross-layer interactions remains a vital direction for future network-layer extensions.

Remark 3 Equation (18) explicitly demonstrates that in the asymptotically high-SNR regime ($\rho \to \infty$), the average BLER decays to zero ($\bar{\epsilon}^{\infty} \to 0$) and the effective system throughput reaches its maximum saturation limit, $\eta \to R_c$. However, the speed at which the system approaches this maximum limit is strictly governed by the physical diversity order S.

3.5 System Reliability

In the context of short-packet communications, system reliability is defined as the probability that a transmitted finite-length packet is successfully decoded and accurately identified at the receiver. Based on the average BLER evaluated in Theorem 1, the overall system reliability of the FAS link can be mathematically expressed as a percentage [35], Eq. (27):

$$\mathcal{R} = (1 - \bar{\epsilon}) \times 100\%. \tag{19}$$

By substituting the exact closed-form expression of the average BLER from (14) into (19), we can directly quantify the exact reliability of the proposed system. Furthermore, utilizing the high-SNR approximations, the asymptotic reliability readily approaches $\mathcal{R}^{\infty} = (1 - \bar{\epsilon}^{\infty}) \times 100\%$, where $\bar{\epsilon}^{\infty}$ is strictly governed by the physical-diversity order S, as derived in (15).

3.6 Optimal Blocklength Allocation for Throughput Maximization

In short-packet communications, the payload size D is typically predetermined by the application layer, whereas the blocklength L serves as a critical design degree of freedom. A smaller L elevates the coding rate $R_c = D/L$, which triggers a sharp growth in the average BLER$\bar{\epsilon}(L)$, thereby severely degrading the effective system throughput. Conversely, an excessively large L ensures low block errors, but causes a drastic penalty in spectral efficiency due to the over-allocation of time-frequency slots. This fundamental conflict motivates the formulation of an optimization problem to find the optimal blocklength L^* that maximizes the effective system throughput under strict latency and reliability boundaries:

$$\begin{aligned} \max_{L} \eta(L) \quad & = \frac{D}{L}(1 - \bar{\epsilon}(L)) \\ \text{s.t. } L_{\min} \quad & \leq L \leq L_{\max} \\ \bar{\epsilon}(L) & \leq \epsilon_{\max} \end{aligned} \tag{20}$$

where $L_{\min}$ and $L_{\max}$ represent the operational latency limits and $\epsilon_{\max}$ denotes the maximum tolerable block error rate. Due to the complex non-linear coupling of L within both the coding rate and the channel dispersion in the average BLER formula (14), obtaining a closed-form derivative with respect to L is mathematically intractable. However, since the objective function $\eta(L)$ is strictly quasi-concave with respect to L, the unique optimal blocklength L^* can be efficiently and reliably extracted *via* low-complexity numerical search schemes, such as the golden-section search or the standard bisection method.

4. NUMERICAL RESULTS

In this section, we provide extensive numerical results to validate our derived analytical expressions and explore the system's behavior. Unless otherwise specified, we set the normalized physical space to $L_s = 1$. For the short-packet parameters, we assume that the transmitter sends an information payload of $D = 120$ bits over a blocklength of $L = 100$ channel uses, yielding a nominal coding rate of $R_c = 1.2$ bpcu. The average transmit SNR ρ varies from -5 dB to 25 dB and the number of fluid ports is evaluated for $K \in \{2,3,4,30\}$. Furthermore, based on the spatial correlation model in (C.5), we generate 10^7 independent random channel realizations to compute the sample mean for all exhaustive Monte Carlo simulation results.

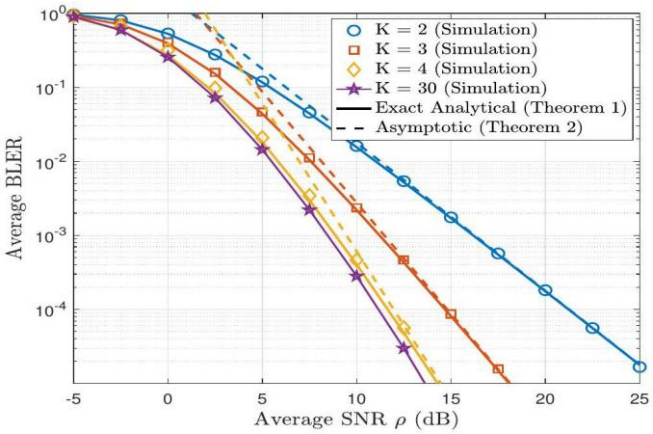


Figure 1. Average BLER *versus* ρ with $L_s = 1$.

In Figure 1, we plot the average BLER *versus* the average transmit SNR ρ for a fixed normalized length $L_s = 1$ with different numbers of fluid ports K. As expected, the average BLER decreases significantly as K increases. The curves exhibit a steeper slope at high SNR regimes, which strictly reflects a higher

diversity order compared to the traditional single-antenna baseline ($K = 1$). However, it is observed that as K grows beyond 4 to a much larger value (e.g., $= 30$), the performance improvement becomes marginal and the curves begin to pack closely together. This behavior perfectly aligns with our theoretical findings in Theorem 2 and the physical intuition discussed in Remark 1. Specifically, the asymptotic analysis mathematically reveals that the diversity order does not scale indefinitely with K, but is fundamentally limited by S, the effective rank of the spatial correlation matrix **R**. For a fixed physical space L_s, packing more ports densely together drastically strengthens the spatial correlation among them. This extreme correlation restricts the rank S and ultimately saturates the achievable diversity order and spatial degrees of freedom for short-packet communications.

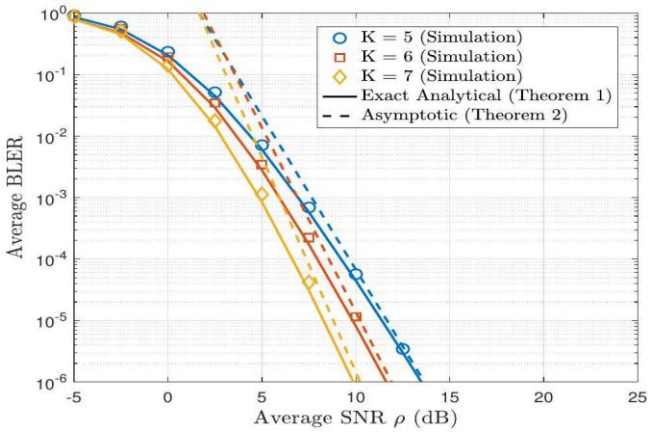


Figure 2. Average BLER *versus* ρ with $L_s = 3$.

To explore the effect of expanding the physical size of the fluid antenna, we plot the average BLER for a larger normalized space of $L_s = 3$ in Figure 2. Compared to the severely constrained space ($L_s = 1$) in Figure 1, expanding the physical dimension allows the K ports to be distributed with significantly reduced spatial correlation. This reduction in correlation inherently increases the effective rank S of the spatial correlation matrix **R**, thereby unlocking a higher effective diversity order. Consequently, as K increases, the average BLER improves even more drastically and each corresponding curve exhibits a noticeably steeper slope. Notably, the performance gap between $K = 4$ and $K = 30$ is much more pronounced here than in Figure 1, indicating that the diversity order has not yet saturated as severely. Furthermore, across both Figure 1 and Figure 2, the exact analytical BLER derived in Theorem 1 (solid lines) matches the exhaustive Monte Carlo simulations (symbols) flawlessly. At the same time, the highSNR asymptotic approximations derived in Theorem 2 (dashed lines) tightly converge with the exact curves in the high-SNR regime. This convergence definitively validates the accuracy of our theoretical derivations and confirms that the diversity order is strictly governed by the rank S.

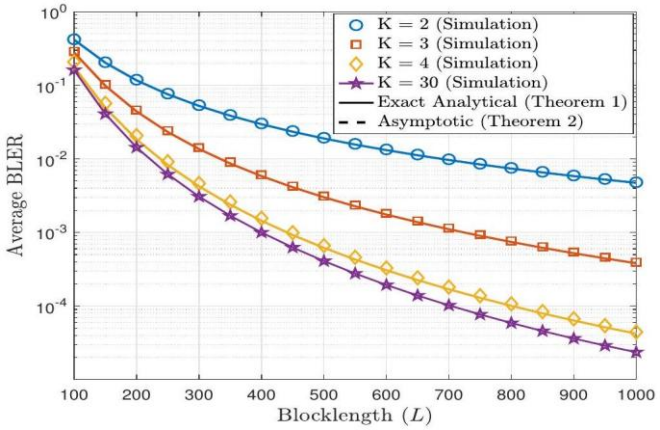


Figure 3. Average BLER *versus* Blocklength L with $L_s = 1$ and $= 1$ dB.

In Figure 3, we investigate the impact of the blocklength L on the average BLER while maintaining a fixed physical space $L_s = 1$ and $K = \{2,3,4,30\}$ ports. As L increases from 100 to 1000 channel uses, the BLER curves shift significantly towards the lower SNR region. This aligns with short-packet

communication principles, where a larger L for a fixed payload D yields a lower effective coding rate R_c, enabling the system to achieve the same reliability target with a lower transmit power.

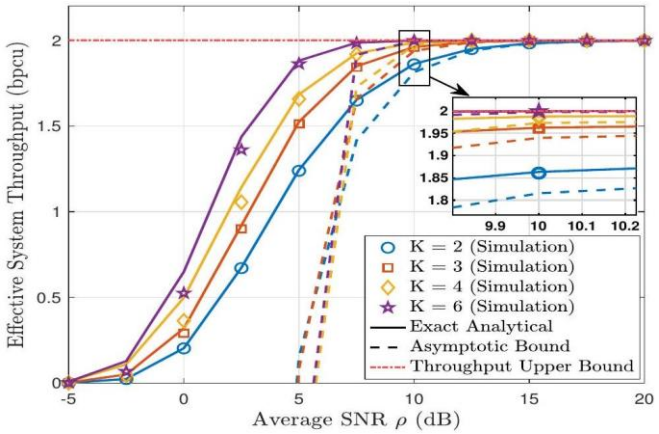


Figure 4. Effective system throughput *versus* ρ with $L_s = 2, D = 200$ bits and $L = 100$.

Figure 4 evaluates the effective system throughput *versus* the average SNR ρ for $L_s = 2, D = 200$ bits and $L = 100$. As expected, the throughput increases monotonically with ρ and eventually saturates at the theoretical upper bound of $R_c = 2.0$ bpcu. Furthermore, deploying a denser FAS configuration (e.g., increasing K to 6) significantly shifts the curves to the left, enabling the system to reach near-maximum throughput at a much lower transmit power. Finally, the exact agreement between the analytical expressions, asymptotic bounds and Monte Carlo simulations firmly validates our throughput derivations in Sub-section 3.3.

Figure 5 illustrates the system reliability *versus* the average SNR ρ for $L_s = 2, D = 200$ bits and $L = 100$. As expected, the reliability monotonically increases with ρ and ultimately saturates at the absolute maximum of 100%. Notably, deploying a denser FAS configuration (e.g., $= 6$) drastically shifts the curves towards the lower SNR region. This demonstrates that a higher number of fluid ports allows the system to guarantee near-perfect packet delivery at a significantly reduced transmit power. Finally, the exact match among the analytical expressions, asymptotic bounds and Monte Carlo simulations rigorously validates our reliability derivations in Sub-section 3.5.

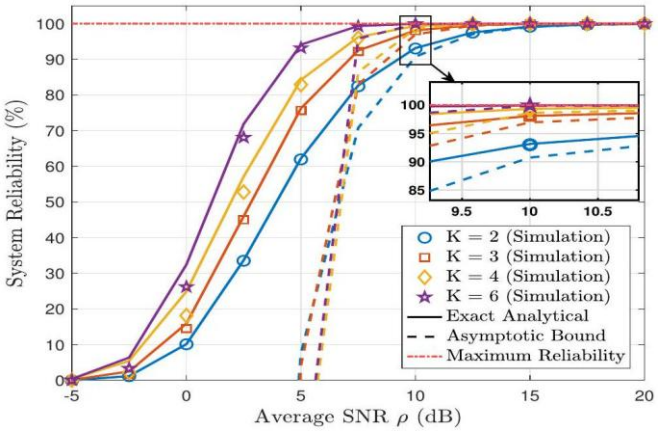


Figure 5. System reliability *versus* ρ with $L_s = 2, D = 200$ bits and $L = 100$.

Figure 8 illustrates the effective throughput η *versus* blocklength L for various numbers of FAS ports $K \in \{2,3,4,30\}$. As observed from the figure, all throughput curves exhibit a distinct single-peak behavior, which numerically validates the quasi-concavity of the objective function with respect to L. When L is relatively small, the throughput drops to zero because the short blocklength cannot combat the severe channel fading, leading to a high BLER. As L increases, the BLER decreases significantly, causing a sharp rise in throughput until it reaches the global maximum at the optimal blocklength L^*, denoted by the red stars. Beyond this optimal point, further increasing L diminishes the transmission rate D/L, thereby resulting in a gradual decline in the effective system throughput. Furthermore, the results highlight the significant advantage of deploying a large number of FAS ports. Specifically,

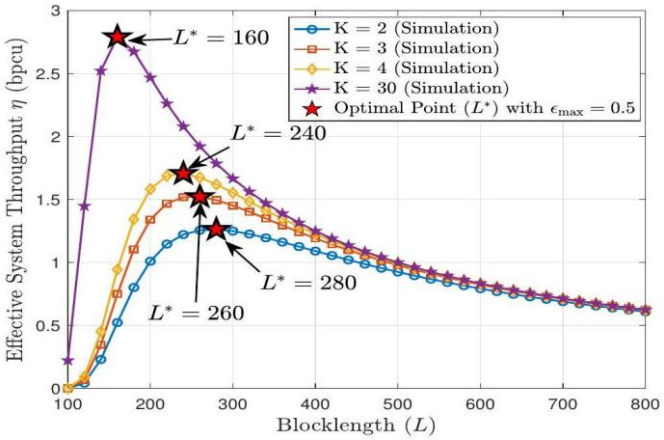


Figure 6. Effective system throughput *versus* blocklength L for $L_s = 3$ and $D = 500$ bits.

increasing K from 2 to 30 drastically enhances the maximum achievable throughput due to the enhanced spatial diversity gain of fluid antennas. Crucially, a larger K shifts the optimal blocklength L^* toward a smaller value (i.e., to the left of the horizontal axis). This indicates that by exploiting the fine-grained port selection in FAS, the system can achieve peak throughput at a much shorter blocklength, effectively minimizing the transmission latency while maintaining high reliability, which is highly desirable for short-packet URLLC systems.

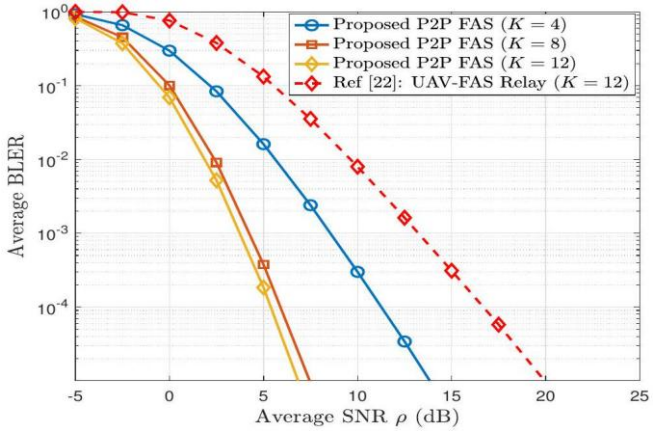


Figure 7. Average BLER *versus* ρ for $L_s = 3, D = 120$ bits and $L = 100$ under the optimistic constant correlation model [23].

Figure 7 illustrates the average BLER *versus* the average SNR ρ for the proposed P2P FAS ($K \in \{3,8,12\}$) alongside the UAV-FAS relay benchmark [23]. As observed, increasing the number of fluid ports from $K = 3$ to $K = 12$ drastically enhances system reliability, shifting the BLER curves to the lower-SNR region.

Crucially, under the same configuration (e.g., $= 12$), our proposed direct architecture significantly outperforms the UAV relay benchmark [23]. The relay topology suffers from a severe half-duplex penalty, which forces a doubled coding rate and heavily degrades decoding accuracy under strict short-packet constraints. By completely bypassing this penalty, our P2P FAS framework proves to be a vastly superior and power-efficient solution for practical URLLC applications.

Finally, Figure 8 illustrates the average BLER performance *versus* the average transmit SNR ρ for both the proposed high-density FAS and the traditional ideal selection combining (SC) schemes under SPC constraints. To establish a realistic benchmark, the spatial dimension is strictly constrained to $L_s = 1$. Within this normalized limited space, traditional SC can deploy at most $K = 3$ co-located antennas to maintain independent fading channel characteristics. As observed from the simulation results, the proposed FAS with $K = 30$ ports significantly outperforms the physical boundaries of the traditional ideal SC ($= 2$ and $K = 3$). Specifically, at a target BLER of 10^{-4}, the proposed FAS achieves approximately a 3 dB SNR gain compared to the maximum bound of the traditional ideal SC($K = 3$). Furthermore, the curves clearly indicate that FAS provides a sharper slope in the high-SNR regime. This

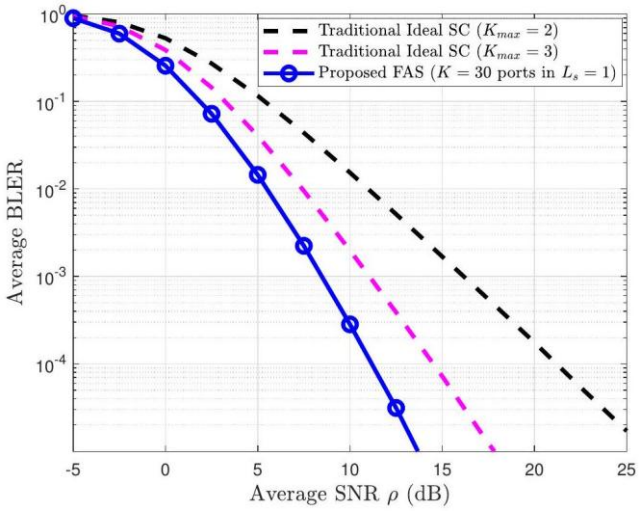


Figure 8. Average BLER *versus* average transmit SNR ρ for the proposed FAS ($K = 30$) and traditional ideal SC ($K = 2,3$) under short-packet transmission constraints ($L_s = 1, D = 120$ bits and $L_{\text{block}} = 100$).

behavior is attributed to the fact that although the ultra-dense port arrangement in FAS introduces severe spatial correlation, the effective rank of the Jakes' correlation matrix over $L_s = 1$ is approximately 4. By deploying $K = 30$ ports, FAS successfully captures all available spatial degrees of freedom and maximizes the array gain through fine-grained selection, whereas traditional SC is fundamentally restricted by hardware and spatial constraints. These findings firmly highlight the superiority of fluid-antenna technology in breaking the physical limits of conventional multi-antenna systems for ultra-reliable low-latency IoT networks.

5. CONCLUSION

In this paper, we rigorously analyzed the delivery performance of FAS under the strict and highly realistic constraints of short-packet communications, departing from the conventional infinite-blocklength Shannon capacity framework. By accurately modeling the heavily correlated spatial fading channels *via* eigenvalue decomposition, we successfully derived highly accurate, closed-form expressions for the exact average BLER, the effective system throughput and the overall system reliability. Furthermore, our high-SNR asymptotic analysis mathematically proved that the diversity order of an FAS link is strictly determined and bounded by the rank of its spatial correlation matrix, rather than the raw number of fluid ports. The comprehensive numerical results flawlessly confirmed our theoretical derivations, highlighting that densely packed FAS configurations can achieve near-perfect reliability and maximum throughput at significantly reduced transmit power levels. Ultimately, these findings demonstrate that FAS is a highly promising architectural solution for meeting the extreme delivery demands of modern IoT and URLLC networks, offering substantial performance leaps without the need for bulky, power-hungry multiple-RFchain hardware typical of traditional multi-antenna setups.

APPENDICES

A. PROOF OF THEOREM 1

By substituting the piecewise linear approximation (10) into the expectation integral (9), we obtain:

$$\bar{\epsilon} \approx \int_0^a 1 \cdot f_\Gamma(x)dx + \int_a^b \left[\frac{1}{2} - \beta(x-\theta)\right] f_\Gamma(x)dx. \tag{A.1}$$

The first term trivially evaluates to $F_\Gamma(a)$. For the second term, we apply integration by parts. Let $u = \frac{1}{2} - \beta(x-\theta)$, yielding $du = -\beta dx$. Let $dv = f_\Gamma(x)dx$, yielding $v = F_\Gamma(x)$. Evaluating the boundaries gives:

$$\left[\frac{1}{2} - \beta(x-\theta)\right] F_\Gamma(x)\Big|_a^b + \beta \int_a^b F_\Gamma(x)dx. \tag{A.2}$$

Due to the symmetric definitions of a and b around θ in (12), the boundary evaluations exactly cancel out the $F_\Gamma(a)$ term. The average BLER simplifies to:

$$\bar{\epsilon} \approx \beta \int_a^b F_\Gamma(x)dx. \tag{A.3}$$

Optionally, substituting the CDF expression from (6) into (A.3) yields:

$$\bar{\epsilon} \approx \beta \int_a^b \left(1 + \sum_{k=1}^{S} (-1)^k \sum_{\mathcal{N}_k} e^{-\frac{x\Delta_k}{\rho}}\right) dx. \tag{A.4}$$

Evaluating the integral of the exponential function, we have:

$$\begin{aligned}\bar{\epsilon} =& \approx \beta(b-a) + \sum_{k=1}^{S} (-1)^k \sum_{\mathcal{N}_k} \beta \int_a^b e^{-\frac{x\Delta_k}{\rho}} dx \\ &= 1 + \sum_{k=1}^{S} (-1)^k \sum_{\mathcal{N}_k} \frac{\beta\rho}{\Delta_k}\left(e^{-\frac{a\Delta_k}{\rho}} - e^{-\frac{b\Delta_k}{\rho}}\right).\end{aligned} \tag{A.5}$$

Note that $\beta(b-a) = 1$ is used in the final step. This completes the proof.

B. PROOF OF THEOREM 2

To uncover the asymptotic behavior ($\rho \to \infty$), we simplify the CDF$F_\Gamma(x)$. The exact CDF before applying the inclusion-exclusion principle is a product of independent exponential variables:

$$F_\Gamma(x) = \prod_{i=1}^{S} \left(1 - e^{-\frac{x}{\rho\mu_i}}\right). \tag{B.1}$$

As $\rho \to \infty$, the term $\frac{x}{\rho\mu_i} \to 0$. Applying the first-order Maclaurin series expansion $e^{-z} \approx 1 - z$, the CDF simplifies to:

$$F_\Gamma^{\infty}(x) \approx \prod_{i=1}^{S} \left(\frac{x}{\rho\mu_i}\right) = \left(\frac{1}{\prod_{i=1}^{S} \mu_i}\right)\left(\frac{1}{\rho}\right)^S x^S. \tag{B.2}$$

Substituting (B.2) into the simplified integral (A.3) gives:

$$\begin{aligned}\bar{\epsilon}^{\infty} &\approx \beta \int_a^b F_\Gamma^{\infty}(x)dx = \beta\left(\frac{1}{\prod_{i=1}^{S} \mu_i}\right)\left(\frac{1}{\rho}\right)^S \int_a^b x^S dx \\ &= \frac{\beta}{S+1}\left(\frac{1}{\prod_{i=1}^{S} \mu_i}\right)\left(\frac{1}{\rho}\right)^S (b^{S+1} - a^{S+1}).\end{aligned} \tag{B.3}$$

This completes the proof.

C. RIGOROUS PROOF OF DIVERSITY ORDER *VIA* CHANNEL BOUNDS

To establish the exact diversity order without relying on any distribution approximation of the SNR, we bound the true combined channel gain $|h_{\mathrm{FAS}}|^2 \triangleq \max_{1\le k\le K} |h_k|^2$. *Via* the eigenvalue decomposition of the spatial correlation matrix $\mathbf{R} = \mathbf{U}\mathbf{\Lambda}\mathbf{U}^H$, the channel vector can be modeled as $\mathbf{h} = \mathbf{U}\mathbf{\Lambda}^{1/2}\mathbf{z}$, where $\mathbf{z} \sim \mathcal{CN}(\mathbf{0}, \mathbf{I}_K)$. The squared norm of the channel vector satisfies $\|\mathbf{h}\|^2 = \sum_{m=1}^{S} \mu_m |z_m|^2$, where $S = \mathrm{Rank}(\mathbf{R})$ and μ_m represents the ordered non-zero eigenvalues. Following the bounding methodology in [29], we utilize the inequality $\frac{1}{K}\|\mathbf{h}\|^2 \le |h_{\mathrm{FAS}}|^2 \le \|\mathbf{h}\|^2$, which yields:

$$\frac{\mu_{\min}}{K} Z \le |h_{\mathrm{FAS}}|^2 \le \mu_{\max} Z, \tag{C.1}$$

where $Z = \sum_{m=1}^{S} |z_m|^2$ is a Gamma-distributed random variable with shape parameter S and scale parameter 1 , while $\mu_{\min}$ and $\mu_{\max}$ denote the minimum and maximum non-zero eigenvalues of $\mathbf{R}$, respectively.

Let $\Gamma = \rho|h_{\mathrm{FAS}}|^2$ be the exact instantaneous SNR. Its true CDF, $F_\Gamma(x)$, is strictly bounded by $F_\Gamma^{\text{lower}}(x) \le F_\Gamma(x) \le F_\Gamma^{\text{upper}}(x)$, where $F_\Gamma^{\text{lower}}(x) = \Pr\left(Z \le \frac{x}{\mu_{\max}\rho}\right)$ and $F_\Gamma^{\text{upper}}(x) = \Pr\left(Z \le \frac{Kx}{\mu_{\min}\rho}\right)$.

By applying integration by parts as detailed in Appendix A, the exact average BLER $\bar{\epsilon}$ under short-packet constraints is expressed as $\bar{\epsilon} = \beta \int_a^b F_\Gamma(x)dx$. Since the operation preserves the inequality directions, we obtain $\bar{\epsilon}^{\text{lower}} \le \bar{\epsilon} \le \bar{\epsilon}^{\text{upper}}$, where $\bar{\epsilon}^{\text{lower}} = \beta \int_a^b F_\Gamma^{\text{lower}}(x)dx$ and $\bar{\epsilon}^{\text{upper}} = \beta \int_a^b F_\Gamma^{\text{upper}}(x)dx$.

In the high-SNR regime ($\rho \to \infty$), the standard Gamma CDF near zero expands asymptotically *via* Maclaurin series as $F_\Gamma^{\text{lower}}(x) \simeq \frac{1}{S!}\left(\frac{x}{\mu_{\max}\rho}\right)^S$ and $F_\Gamma^{\text{upper}}(x) \simeq \frac{1}{S!}\left(\frac{Kx}{\mu_{\min}\rho}\right)^S$. Substituting these polynomial expansions back into the integrals, both the upper and lower bounds of the average BLER converge to the identical mathematical order of $\mathcal{O}(\rho^{-S})$. Finally, invoking the Squeeze Theorem, the exact diversity order d is rigorously established as:

$$d = -\lim_{\rho\to\infty} \frac{\ln \bar{\epsilon}}{\ln \rho} = S = \mathrm{Rank}(\mathbf{R}). \tag{C.2}$$

This completes the mathematically rigorous proof and demonstrates that the asymptotic behavior is unaltered by the distribution approximation.

REFERENCES

[1] B. Hassan, S. Baig and M. Asif, "Key Technologies for Ultra-reliable and Low-latency Communication in 6G," IEEE Communications Standards Magazine, vol. 5, no. 2, pp. 106-113, 2021.

[2] M. Adhikari and A. Hazra, "6G-enabled Ultra-reliable Low-latency Communication in Edge Networks," IEEE Communications Standards Magazine, vol. 6, no. 1, pp. 67-74, 2022.

[3] T. Q. Duong, D. Van Huynh, S. R. Khosravirad, V. Sharma, O. A. Dobre and H. Shin, "From Digital Twin to Metaverse: The Role of 6G Ultra-reliable and Low-latency Communications with Multitier Computing," IEEE Wireless Communications, vol. 30, no. 3, pp. 140-146, 2023.

[4] X. Zhao, J. Liu, Y. Wang and J. Wang, "CryptoMamba-SSM: Linear Complexity State Space Models for Cryptocurrency Volatility Prediction," IEEE Open J. of the Computer Society, vol. 7, pp. 226-243, 2026.

[5] Y. Zhu, Y. Hu, X. Yuan, M. C. Gursoy, H. V. Poor and A. Schmeink, "Joint Convexity of Error Probability in Blocklength and Transmit Power in the Finite Blocklength Regime," IEEE Transactions on Wireless Communications, vol. 22, no. 4, pp. 2409-2423, 2023.

[6] M. Yin, Y. Yang, J.-M. Wu and B. Jiao, "Opportunistic Bits in Short-packet Communications: A Finite Blocklength Perspective," IEEE Transactions on Communications, vol. 69, no. 12, pp. 80858099, 2021.

[7] C. Feng, H.-M. Wang and H. V. Poor, "Reliable and Secure Short-packet Communications," IEEE Transactions on Wireless Communications, vol. 21, no. 3, pp. 1913-1926, 2022.

[8] C. M. W. Basnayaka, D. N. K. Jayakody, T. D. P. Perera and M. Beko, "DataAge: Age of Information in SWIPT-driven Short Packet IoT Wireless Communications," IEEE Internet of Things Journal, vol. 11, no. 16, pp. 26984-26999, 2024.

[9] F. A. Pereira de Figueiredo, "An Overview of Massive MIMO for 5G and 6G," IEEE Latin America Transactions, vol. 20, no. 6, pp. 931-940, 2022.

[10] H. Q. Ngo, G. Interdonato, E. G. Larsson, G. Caire and J. G. Andrews, "Ultradense Cell-free Massive MIMO for 6G: Technical Overview and Open Questions," Proceedings of the IEEE, vol. 112, no. 7, pp. 805-831, 2024.

[11] N. T. Nguyen, V.-D. Nguyen, H. V. Nguyen, H. Q. Ngo, A. L. Swindlehurst and M. Juntti, "Performance Analysis and Power Allocation for Massive MIMO ISAC Systems," IEEE Transactions on Signal Processing, vol. 73, pp. 1691-1707, 2025.

[12] Y. Lu, J. Zhang, E. Shi, P. Zhang, D. W. Kwan Ng, D. Niyato and B. Ai, "Energy-efficient RIS-Aided Cell-free Massive MIMO Systems: Application, Opportunities and Challenges," IEEE Wireless Communications, vol. 32, no. 4, pp. 148-155, 2025.

[13] B. Di, H. Zhang, Z. Han, R. Zhang and L. Song, "Reconfigurable Holographic Surface: A New Paradigm for Ultra-massive MIMO," IEEE Transactions on Cognitive Communications and Networking, vol. 11, no. 6, pp. 3761-3783, 2025.

[14] T. C. Rapudu and O. O. Oyerinde, "Machine Learning-based Channel Estimation for Multi-RIS-assisted mmWave Massive-MIMO OFDM System in a Dynamic Environment," IEEE Transactions on Wireless Communications, vol. 24, no. 6, pp. 5297-5309, 2025.

[15] K. N. Le, "Impact of Fading Correlation and Finite-blocklength Regimes on Secrecy," IEEE Transactions on Vehicular Technology, vol. 72, no. 3, pp. 4068-4072, 2023.

[16] C. Psomas, P. J. Smith, H. A. Suraweera and I. Krikidis, "Continuous Fluid Antenna Systems: Modeling and Analysis," IEEE Communications Letters, vol. 27, no. 12, pp. 3370-3374, 2023.

[17] C. Wang, Z. Li, K.-K. Wong, R. Murch, C.-B. Chae and S. Jin, "Ai-empowered Fluid Antenna Systems: Opportunities, Challenges and Future Directions," IEEE Wireless Communications, vol. 31, no. 5, pp. 34-41, 2024.

[18] W. K. New, K.-K. Wong, C. Wang, C.-B. Chae, R. Murch, H. Jafarkhani and Y. Hao, "Fluid Antenna Systems: Redefining Reconfigurable Wireless Communications," IEEE Journal on Selected Areas in Communications, vol. 44, pp. 1013-1044, 2026.

[19] T. Gong, P. Gavriilidis, R. Ji, C. Huang, G. C. Alexandropoulos, L. Wei, Z. Zhang, M. Debbah, H. V. Poor and C. Yuen, "Holographic MIMO Communications: Theoretical Foundations, Enabling Technologies and Future Directions," IEEE Communications Surveys & Tutorials, vol. 26, no. 1, pp. 196-257, 2024.

[20] K.-F. Tong, B. Liu and K.-K. Wong, "Designs and Challenges in Fluid Antenna System Hardware," Electronics, vol. 14, no. 7, [Online], Available: https://www.mdpi.com/2079-9292/14/7/1458, 2025.

[21] D. Bepari, S. Mondal, A. Bhowal, K. Singh, H. Shin, K.-K. Wong and D. W. K. Ng, "Fluid Antennas: Pioneering a New Era in Next-generation Wireless Communications," IEEE Communications Surveys & Tutorials, vol. 28, pp. 5596-5631, 2026.

[22] P. Ramírez-Espinosa et al., "A New Spatial Block-correlation Model for Fluid Antenna Systems," IEEE Trans. on Wireless Communications, vol. 23, no. 11, pp. 15829-15843, 2024.

[23] X. Zhu et al., "UAV-enabled Short-packet Communication *via* Fluid Antenna Systems," arXiv: 2602.06206, DOI: 10.48550/arXiv.2602.06206, 2026.

[24] Z. Zhang et al., "Finite-blocklength Fluid Antenna Systems," arXiv: 2509.15643**,** [Online], Available: https://arxiv.org/abs/2509.15643, 2026.

[25] X. Zhu et al., "Fluid Antenna Systems: A Geometric Approach to Error Probability and Fundamental Limits," IEEE Trans. on Wireless Communications, vol. 25, pp. 17195-17209, 2026.

[26] X. Zhu et al., "Fluid Antenna Systems Enabling 6G HRLLC with Port Switching Delay," arXiv: 2605.06275, [Online], Available: https://arxiv.org/abs/2605.06275, 2026.

[27] X. Zhu et al., "Fluid Antenna System-enabled UAV Communications in the Finite Blocklength Regime," IEEE Transactions on Wireless Communications, vol. 25, pp. 16714-16729, 2026.

[28] G. L. Stüber, Principles of Mobile Communication, 4th Edn, ISBN: 978-3-319-55615-4, Springer Nature, 2017.

[29] H. Zhao and D. Slock, "Analytical Insights into Outage Probability and Ergodic Capacity of Fluid Antenna Systems," IEEE Wireless Communications Letters, vol. 14, no. 5, pp. 1581-1585, 2025.

[30] M. Khammassi et al., "A New Analytical Approximation of the Fluid Antenna System Channel," IEEE Trans. on Wireless Communications, vol. 22, no. 12, pp. 8843-8858, 2023.
[31] W. K. New et al., "Fluid Antenna System: New Insights on Outage Probability and Diversity Gain," IEEE Trans. on Wireless Communications, vol. 23, no. 1, pp. 128-140, 2024.
[32] T.-H. Vu, T.-V. Nguyen, Q.-V. Pham, D. Benevides da Costa and S. Kim, "STAR-RIS-enabled Short-packet NOMA Systems," IEEE Trans. on Vehicular Technology, vol. 72, no. 10, pp. 13764-13769, 2023.
[33] T.-T. T. Nguyen, X.-X. Nguyen and N. V. T. Nguyen, "Short-packet Communications for Pinching-antenna Systems," IEEE Communications Letters, vol. 30, pp. 1270-1274, 2026.
[34] L. T. T. Huyen, B. A. Duc, X. N. Tran, B. C. Nguyen, L. T. Dung and T. M. Hoang, "BLER and BER Performance of RSMA in Multi-antenna Systems over Nakagami Fading Channels," IEEE Internet of Things Journal, Early Access, DOI: 10.1109/JIOT.2026.3686852, 2026.
[35] G. N. Tran and S. Kim, "Performance Analysis of Short Packets in NOMA VLC Systems," IEEE Access, vol. 10, pp. 6505-6517, 2022.

ملخص البحث:

توفّر أنظمة الهوائيات المائعة تنوُّعاً مكانياً هائلاً ضمن مساحاتٍ مُدمجة. ومع ذلك، فإنّ تحليلات الأداء الحالية تعتمد في الغالب على حُدود سِعة "شانون"، بافتراض إرسال كُتل بياناتٍ ذات طولٍ لا نهائي. ولتلبية المتطلّبات الصّارمة لتطبيقات إنترنت الأشياء، تبحث هذه الورقة في نظام هوائياتٍ مائعة يعمل بنمط الاتّصال من نقطةٍ إلى نقطةٍ في ظلّ قيود الاتّصالات ذات الحُزم القصيرة.

يتمّ اشتقاق دقيق لِصيغ تحليلية مغلقة تعبّر عن متوسّط معدّل خطأ الكتلة، والإنتاجية الفعلية للنّظام، والموثوقية. كذلك نجري تحليلاً تقاربياً في نطاق نسبة الإشارة إلى الضّوضاء العالية، ونكشف رياضياً أنّ رُتبة التّنوّع في النّظام تتحدّد بشكلٍ صارمٍ بناءً على رتبة مصفوفة الارتباط المكاني.

وتبيّن محاكاة مونت كارلو الدّقة العالية للنّماذج التّحليلية، حيث تؤدي زيادة عدد المنافذ المائعة إلى خفض معدّل خطأ الكتلة بشكلٍ ملحوظ.

This article is an open access article distributed under the terms and conditions of the Creative Commons Attribution (CC BY) license (http://creativecommons.org/licenses/by/4.0/).